Magnesium Technology 2012
Edited by: Suveen N. Mathaudhu, Wim H. Sillekens, Neale R. Neelameggham, and Norbert Hort
TMS (The Minerals, Metals & Materials Society), 2012

STRAIN-RATE EFFECTS OF SAND-CAST AND DIE-CAST MAGNESIUM ALLOYS UNDER COMPRESSIVE LOADING

J.P. Weiler[1], J.T. Wood[1]

[1] Department of Mechanical and Materials Engineering, University of Western Ontario, London, Canada, N6A 5B9

Keywords: Compressive impact testing; Strain-rate effects; Cast magnesium alloys; Constitutive modeling

Abstract

The strain-rate effects of cast magnesium alloys were investigated with uniaxial compression and compressive impact testing. The compressive material response of specimens cut from sand cast AZ91, AE44, and AM60, and high-pressure die-cast AM60 was determined for strain-rates ranging from quasi-static levels to typical rates experienced during crash situations. Several different constitutive material models (Johnson-Cook, Cowper-Symonds, etc.) were used in an attempt to characterize the experimental results. These material models are typically available in commercial finite-element packages and can be used to model the resulting material response of die-cast automotive components produced with these alloys to more complex loading conditions. The resulting deformed microstructures and fracture surfaces of each alloy at different strain-rates were also analyzed.

Introduction

Magnesium alloys are increasingly being employed in the automotive industry in a variety of different applications due to their excellent specific strength, ease of castability and potential for reductions in fuel consumption. Automotive components varying from instrument panel beams, steering wheel armatures and seat frames (AM60), to cam covers, clutch housings and steering wheels (AZ91), to high-temperature applications such as engine cradles (AE44) have been manufactured with cast magnesium alloys [1]. With increasing use of, and diversity of components, the response of these alloys to mechanical and dynamic loading must be fully understood. With an understanding of the material behaviour to these loading conditions, comprehensive material models can be developed in numerical simulation packages to characterize the structural behaviour of magnesium alloys. The material behaviour at increased strain-rates, or the crashworthiness of these alloys is of importance to the automotive industry to optimize the use of cast magnesium alloys in the automobile, and facilitate progress in achieving these material models. The crashworthiness of automotive materials can be characterized at a laboratory-scale by performing compression or impact testing at speeds in the range of 1-3 m/s. These tests are capable of deforming specimens at strain rates greater than $100s^{-1}$, approximating the conditions of automobile crashes; a 100 mm component compressed in a car crash at 50km/h realizes a strain-rate of approximately $140s^{-1}$.

In this work, the strain-rate effects of specimens from sand cast AE44, AZ91, and AM60, and high-pressure die-cast AM60 plates were investigated. Uniaxial compression testing and compressive impact testing were performed to achieve strain-rates ranging from $0.0002s^{-1}$ to $490s^{-1}$. Constitutive material models available in structural numerical packages were compared with the results. The resulting microstructures from these quasi-static and dynamic tests were compared with undeformed microstructures of each alloy.

Strain-rate sensitivity in Mg alloys

Several researchers have investigated the strain-rate effects of cast magnesium alloys during both tensile and compressive loading at varying strain-rates [2-7]. These researchers find that both alloy content and grain size influence the strain-rate sensitivity of magnesium alloys. Increases in the aluminum content [2,4,8] and grain size [6] decreases the strain-rate sensitivity of magnesium-based alloys for strain-rates ranging from quasi-static levels to $10s^{-1}$. In this range of strain-rates, the strain-rate sensitivity of AZ91 is considered nearly negligible [2,4], while the strain-rate sensitivity of magnesium alloys with 2% aluminum content – AS21 and AM20 – is considered significant [4-5]. Conversely, small additions of the rare-earth element gadolinium to pure magnesium results in no affect to the tensile strain-rate sensitivity of pure magnesium at strains up to $10s^{-1}$, and the elongation values of the binary alloy are unaffected by increases in the strain-rate [7]. At a range of greater strain-rates, $15s^{-1}$ to $130s^{-1}$, the ultimate tensile strength of AM50, AM60 and AZ91 magnesium alloys increases, indicating a positive strain-rate sensitivity of each of these alloys [3]. At a strain-rate of approximately $1700s^{-1}$, the compressive ultimate stress values of magnesium alloys AM20, AM50 and AM60 increase, while the elongation values decrease compared with measured values at a strain-rate of $1s^{-1}$ [5]. The strain-rate sensitivity of AM20 was found to be the greatest; indicating that even at these large strain-rates, the strain-rate sensitivity of magnesium alloys is influenced by the aluminum content [5].

Dynamic constitutive material models

Numerous constitutive material models characterizing strain-rate effects are available in literature and available for in numerical packages, such as LS-DYNA [8]. LS-DYNA implements several of these in the available library of material models including the Johnson-Cook model [9], the Cowper-Symonds model [10], and the Zerilli-Armstrong model [11-12], among others. The Johnson-Cook constitutive material model is based upon torsion and tension tests of fifteen different metals (copper, steel, etc.) at different strain rates and temperatures. This material model defines the flow stress, σ, of a material as [9]:

$$\sigma = \left(A + B\varepsilon_p{}^n\right)\left(1 + C\ln\frac{\dot{\varepsilon}}{\dot{\varepsilon}_o}\right)\left(1 - T^{*m}\right) \quad (1)$$

where: ε_p is the plastic strain, $\dot{\varepsilon}$ is the strain rate, $\dot{\varepsilon}_o$ is the reference strain rate (usually $1s^{-1}$), T^* is the homologous temperature, and the parameters A, B, C, m and n are experimentally determined constants. The quasi-static flow curve of a material can be characterized using A as the yield strength, and $B\varepsilon_p^n$ as the plastic portion of the flow curve. Aune et al. [3] determine Johnson-Cook parameters for die-cast AZ91D, AM50A and AM60B magnesium alloys. They report values of C, the strain-rate sensitivity parameter, of 0.019 for AZ91D and AM50A, and 0.023 for AM60B. Altehnof and Ames [13] use the material parameters reported by Aune et al. in numerical simulations of the impact of an AM50 steering wheel armature. They find that the strain-rate effect is a minimal contribution to the rate of deformation of the material at the strain-rates investigated.

The Cowper-Symonds constitutive material model is based upon bending impact tests of cantilever beams with a mass on one end. This material model defines the flow stress of a material due to increased strain-rate, as [10]:

$$\sigma = \sigma_o + \left(\frac{\dot{\varepsilon}}{D}\right)^{1/p} \tag{2}$$

where: σ_o is the quasi-static reference stress, and D and p are experimental determined material constants. The material constant D is the strain-rate at which the flow stress is twice the quasi-static reference stress. Song, Beggs, and Easton [5] propose the material parameters D and p for several die-cast magnesium alloys including AM60. They report that $D = 3300s^{-1}$ and $p = 1.1$. These researchers also report, however, that the Cowper-Symonds constitutive model does not characterize magnesium alloys well at strain-rates greater than $1000s^{-1}$, as it does not account for the strain-rate sensitivity of the work-hardening behaviour of these alloys.

The Zerilli-Armstrong material model [11] is a 'dislocation-mechanics' based constitutive equation building upon the analysis and data presented by Johnson and Cook [9]. Zerilli and Armstrong give equations for the flow stress of face-centered cubic (FCC) and body-centered cubic (BCC) metals in Ref. [11]. They report in Ref. [12] that since the flow curves of hexagonal close-packed (HCP) metals, such as magnesium alloys, are somewhere between FCC and BCC metals, the dislocation-mechanics based constitutive equation for HCP metals is characterized by a combination of interactions predominant in BCC and FCC metals. However, as of the writing of this paper, the material model library available in LS-DYNA [8] only includes constitutive equations for the flow stress for BCC and FCC metals. The Zerilli-Armstrong constitutive material model defines the flow stress of a BCC material, for example, as [11]:

$$\sigma = c_1 + c_2 \exp\left(-c_3 T + c_4 T \ln \dot{\varepsilon}\right) + c_5 \varepsilon^n \tag{3}$$

where: c_1, c_2, c_3, c_4 and c_5 are experimentally determined constants, T is the ambient temperature, and $c_1 + c_5\varepsilon^n$ characterizes the quasi-static flow curve (in this work, we use similar values of c_3 and c_4 as those reported in [11]).

Experimental Procedures

Materials. The sand casting was performed at CANMET-MTL, in Ottawa, Canada with three different commercially available magnesium alloys: AM60, AZ91 and AE44. The sand casting experiments resulted in a step-casting measuring 330 mm in length, 100 mm in width, and thicknesses of increasing steps, ranging from 4 mm to 40 mm at the feeding riser (Figure 1). The 4 mm step of these castings was used in other studies [14-15]. For compressive and impact testing, rectangular specimens were cut from the nominally 8 mm thick step measuring 5 mm x 5 mm in cross-sectional area (Figure 1). This region of the casting solidified at a rate of approximately 0.5 °C/s, producing grain sizes in the range of 30-50 μm [15].

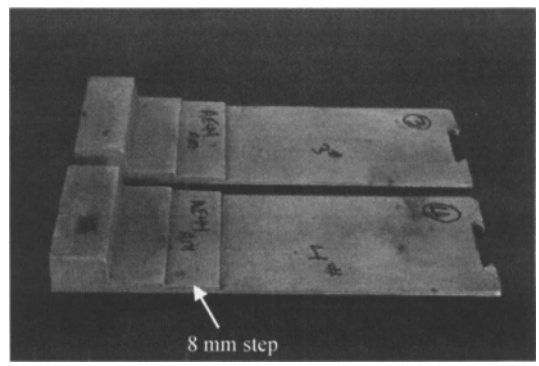

Figure1: AE44 step-plates produced by sand-casting. Specimens were cut from the 8 mm thick step.

The high-pressure die-cast AM60 (HPDC-AM60) test plates were cast at Meridian Lightweight Technologies, in Strathroy, Canada. Rectangular specimens measuring 5 mm x 5 mm in cross-sectional area were cut from the nominally 3 mm casting thickness of the test plates. The chemical composition of each of the alloys investigated is given in Table 1.

Quasi-static and dynamic testing. Uniaxial compression testing was completed on an Instron 8804 load frame with two parallel steel plates until fracture. The crosshead speed was used to determine the initial strain-rate of each test. The tests were completed over three or four magnitudes of strain-rate ranging from $0.0002s^{-1}$ to $0.2s^{-1}$. The strain was calculated from the crosshead displacement corrected for machine compliance. The absorbed energy was calculated using the central difference method on each compressive stress-strain curve.

Compressive impact testing was completed on an Instron Dynatup 9250HV instrumented impact drop tower with a maximum dynamic force of 44 kN. During each test, the time, deflection, velocity, change in kinetic energy, and force of the impactor were recorded. To obtain the widest range of strain-rates, impact tests were performed: 1) at the minimum velocity (approximately 0.8 m/s) with sufficient mass to ensure fracture of the specimen, and 2) with the minimum mass possible at sufficient velocity to ensure fracture. Additional tests were completed at velocities between the velocities of 1) and 2). At least six compression and impact tests were performed at each strain-rate to realize statistical significance.

Table 1: Chemical composition, in weight percentages, of AM60, AZ91 and AE44 magnesium alloys (the Re component in AE44 is a combination of the rare earth elements Ce, La, Nd, and Pr).

Alloy	Mg	Al	Zn	Mn	Si	Cu	Fe	Ni	Be	Re
AM60	93.6	6.1	-----	0.32	0.005	0.001	0.001	0.001	0.001	-----
AZ91	90.3	8.7	0.77	0.23	0.006	0.002	0.002	0.002	0.001	-----
AE44	92.4	3.7	0.01	0.20	0.004	0.001	0.000	0.001	0.001	3.8

Specimen Analysis and Metallography. During impact testing, an AOS Technologies Motionscope M3 high-speed video camera was used to capture the deformation and fracture process of several of the specimens of each alloy at different strain-rates. High-speed video of the impact test was captured at rates of 1000, 2000, 4000 and 8000 frames per second for several of the magnesium alloy specimens. Each frame captured during an impact test was correlated to the corresponding stage of mechanical deformation.

Following testing, the microstructures and fracture surfaces of the typical specimens from each strain-rate and alloy were analyzed and compared with the microstructure of undeformed specimens. Specimens were cold-mounted in an epoxy mount, and successively ground with 180, 400, and 1200 silicon carbide grit paper. The specimens were then finely polished in a slurry of first 0.3μm, and then 0.05μm, alumina. The grain-structure of each specimen was revealed with an etchant consisting of 75 mL of distilled water, 25 mL of glycol and 1 mL of nitric acid.

Experimental Results

Uniaxial compression and impact testing was performed on the sand-cast alloys (AM60, AE44 and AZ91) with the 8mm length of the specimen parallel to the direction of loading. The testing was performed on the high-pressure die-cast AM60 alloy with the 3mm thickness in both parallel and perpendicular orientations to the loading direction, to investigate the effects of the skin region on the mechanical properties and to obtain a wide range of strain-rates using the impact drop tower.

Compression Testing. Uniaxial compression testing was performed at low strain-rates ($0.0001s^{-1}$ to $0.01s^{-1}$) to establish the quasi-static compressive response of these alloys, and at strain rates of approximately $0.1s^{-1}$ to investigate effects of small increases in the strain-rate. Table 2 shows the average yield strength (for HPDC-AM60 specimens; the yield strength of the sand cast alloys is approximately 50 MPa [14], and was not easily determined during impact testing due to the initial inertial load peak), ultimate compressive strength, fracture strain, and absorbed energy for each of the magnesium alloy specimens at the strain-rates investigated. The fracture strain and absorbed energy, for the purpose of this study, were defined as the strain or energy value at the maximum load or point of crack initiation. The fracture of the specimen subsequently occurred with growth of the crack(s).

Table 2 shows that there is no significant increase in the ultimate compressive strength or fracture strain (and as a result, absorbed energy) over the 3 or 4 magnitudes of strain-rates investigated for each alloy, although there is a small increase in ultimate compressive strength for AE44 at a strain-rate of $0.1s^{-1}$. The table also shows that there is an increase in yield strength, a minimal decrease in fracture strain, and essentially no change in ultimate compressive strength for the HPDC-AM60 specimens with the skin region parallel to the loading direction. The differences are possibly due to the influence of the skin region under direct axial compression. Although not shown, the absorbed energy was also determined for each specimen at final fracture of the specimen. These results indicated that the fracture process geometry of the specimen contributes to this measure of absorbed energy. HPDC-AM60 specimens with a 3mm initial height (perpendicular) resulted in two shear cracks meeting in a '*V*', while HPDC-AM60 specimens with a 5mm initial height (parallel) resulted in one shear crack. The sum of these crack lengths was directly proportional to the difference in absorbed energy between the two specimen geometries. As a result, we focus our attention on the initiation of fracture for this study. The results shown in Table 2 were used to determine the typical quasi-static response to compare with impact testing results at increased strain-rates ($>100s^{-1}$).

Impact Testing. The signal recorded by the impact testing equipment contains oscillations in the load versus time output curves due to mechanical resonance and an initial load spike due to inertia loading. Using filtering techniques, the mechanical properties of the specimen under impact loading can be calculated from the load signal [16]. Further, the resulting images from the high-speed video captured of the impact event were used to validate the filtering process. Figure 2 shows the stress-strain curve of an unfiltered signal and the resulting filtered signal of a HPDC-AM60 magnesium alloy specimen under a strain rate of $165s^{-1}$. The figure also shows high-speed video images corresponding to the mechanical response, recorded at 4000 frames per second.

Figure 2 shows the initial load peak due to inertia and the mechanical resonance resulting in several oscillations. The filtered signal smooths these oscillations and ignores the initial interial load peak. Figure 2 also shows images captured from high-speed video characterizing the deformation and fracture of the HPDC-AM60 specimen. The time stamp of these images corresponds with the load signal captured by the drop tower equipment. The crack visible in Figure 2-iii corresponds to the decreasing load values. Figure 2 also shows an increase in the ultimate compressive stress, fracture strain (and absorbed energy) when compared with the quasi-static mechanical propreties given in Table 2 (HPDC-AM60 parallel specimens).

Table 2: Average mechanical properties from uniaxial compression testing of the magnesium alloys.

Alloy	Strain-rate (s^{-1})	Yield Strength (MPa)	Ultimate Compressive Strength (MPa)	Fracture Strain	Absorbed Energy (MJ/m^3)
AM60	0.0002		290.6	0.150	30.4
	0.002		287.7	0.145	29.4
	0.02		288.3	0.153	30.8
	0.1		293.8	0.139	28.0
AZ91	0.0002		293.8	0.135	26.6
	0.002		298.6	0.135	27.7
	0.02		302.9	0.146	30.6
	0.1		293.1	0.132	25.6
AE44	0.0002		239.0	0.135	21.5
	0.002		239.5	0.122	18.9
	0.1		248.8	0.121	20.1
HPDC-AM60 perpendicular	0.002	141.2	372.3	0.149	37.8
	0.02	142.0	377.1	0.152	38.8
	0.2	144.4	372.8	0.142	36.5
HPDC-AM60 parallel	0.001	148.8	370.7	0.130	33.0
	0.01	154.7	375.5	0.135	35.8
	0.1	153.6	376.5	0.134	35.4

Microstructure and Deformation. The microstructure and deformation of the magnesium alloy specimens were investigated using high-speed video of the impact testing and metallography of specimens of typical results for each strain-rate to compare with the undeformed microstructures. High-speed video analysis shows that a small amount of specimen barreling occurs while the specimen is under load (Figure 2-ii), and compression and subsequent fracture occur due to the initiation and growth of shear cracks (Figure 2-iii). The high-speed video analysis also shows evidence of two shear cracks meeting in a *'V'* for the HPDC-AM60 specimens with an initial height of 3mm. Metallographic techniques on the magnesium alloys reveal that at increasing strain-rates, a larger number of small shear cracks appear in the specimen. At quasi-static rates, typically, the specimen contains only the crack that fractures the specimen. The microstructure of quasi-static specimens also reveals minimal shear banding at the fracture surfaces. However, at increasing strain-rates of approximately $250s^{-1}$, there is evidence of several shear bands in the deformed microstructures of several of the specimens, predominantly near the shear cracks (Figure 3).

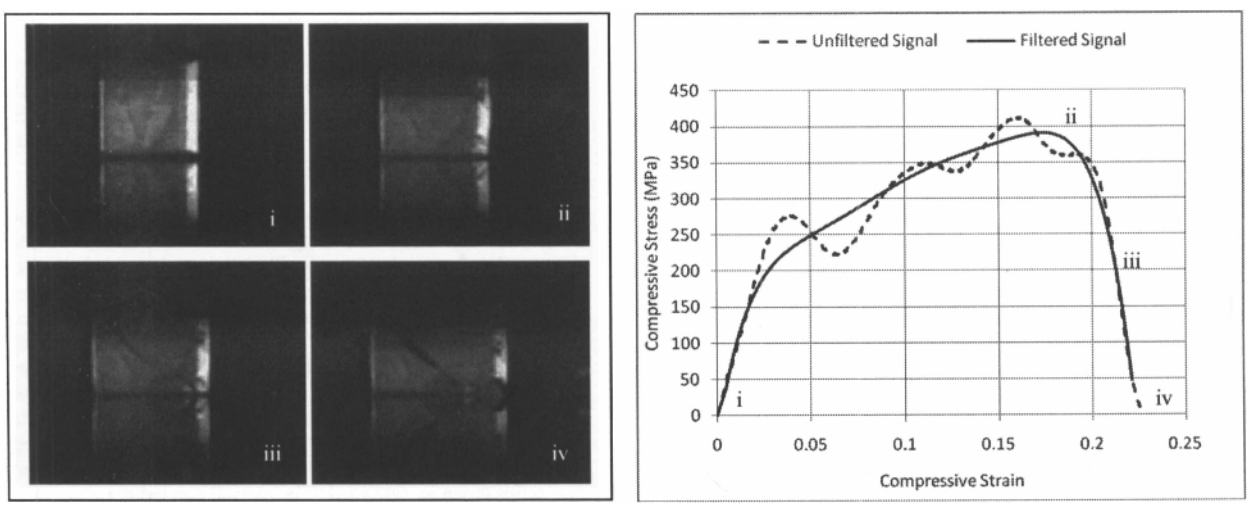

Figure 2: Compressive stress-strain curve of the unfiltered and filtered signal for a HPDC-AM60 specimen under an impact load at a strain rate of $165s^{-1}$, and corresponding images captured from high-speed video showing the deformation and fracture of the specimen.

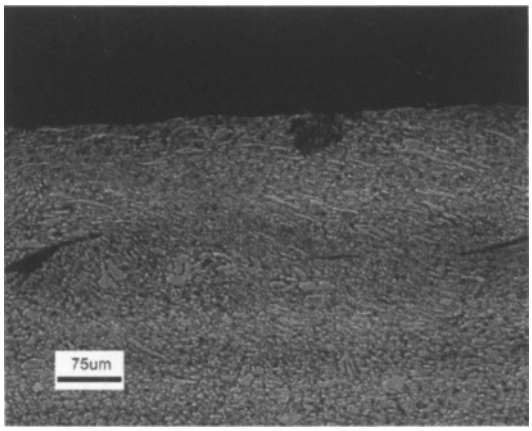

Figure 3: Optical microscope image of shear bands visible in the deformed microstructure of a HPDC-AM60 specimen following impact testing at a strain-rate of $300s^{-1}$ (X200).

Discussion

The impact testing results indicate greater values of the ultimate compressive strength at increased strain-rates compared with the quasi-static values in Table 2 (i.e. Figure 2). We attempt to characterize this increase of these magnesium alloys with the constitutive models given in Equations (1) – (3) found in typical numerical simulation packages, such as LS-DYNA. The flow stress characterized by each of these constitutive models at increased strain-rates can be normalized to the quasi-static reference stress either by division (Johnson-Cook and Cowper-Symonds), or subtraction (Zerilli-Armstrong). As a result, we can investigate the *increase* in ultimate compressive strength from the quasi-static values given in Table 2 due to strain-rate effects. Figure 4 shows the normalized compressive strength (impact compressive strength /quasi-static compressive strength) plotted as a function of strain-rate for each specimen (the HPDC-AM60 data for specimens with the skin region perpendicular and parallel to the loading direction are plotted as one data set). Figure 4 shows that at strain-rates of approximately $100s^{-1}$, the data indicates that the compressive strength increases by approximately 2-3% for each alloy. However, the experimental scatter in the ultimate compressive strengths shown in Figure 4 precludes any definitive evaluation of the data at this strain-rate.

Figure 4 also shows that at strain-rates up to $200s^{-1}$, there is no significant increase in the compressive strength of sand-cast AE44 specimens. Although not shown, there was also no significant increase in fracture strain or absorbed energy at these strain-rates for this alloy. The lack of strain-rate sensitivity for this rare-earth magnesium alloy may be due to the rare-earth alloying elements, as reported in Ref. [7], or the larger grain sizes found in sand castings, as reported in Ref. [6], or a combination of both factors. Further investigation into the relationships between the strain-rate sensitivity of this alloy and the alloying content and grain size is ongoing.

Figure 4 shows that for the sand cast AZ91 alloy, at strain-rates up to $300s^{-1}$, there is an increase of approximately 4%, while for the sand cast AM60 alloy, at strain-rates up to $250s^{-1}$, there is an increase of approximately 3% in the ultimate compressive strengths compared with the quasi-static values. Similar increases were observed for the absorbed energies of these alloys. The figure further shows that the increases in compressive strength for the HPDC-AM60 alloy are greater in magnitude than the sand cast AM60 alloy at similar strain-rates, and increase to approximately 14% at a strain-rate of $490s^{-1}$. Absorbed energy values at these strain rates are also greater. The discrepancy between the HPDC-AM60 and sand cast AM60 sensitivity to strain-rate is possibly due to the differences in grain sizes between these two casting methods [6]. However, further work with a wider range of grain sizes is required to determine any definitive relationship between the strain-rate sensitivity and grain size of cast AM60.

The constitutive models presented in Equations (1) – (3) were used with strain-rate sensitivity parameters of AM60 from literature – a Johnson-Cook parameter of $C = 0.023$ from Aune et al. [3], and Cowper-Symonds parameters of $D = 3300s^{-1}$ and $p = 1.1$ from Song, Beggs, and Easton [5] – in an attempt to characterize the effects of strain-rate on the compressive strength of this magnesium alloy. We restrict our analysis to AM60 due to the number and range of strain-rates at which we were able to perform tests. The parameters for the Zerilli-Armstrong constitutive model are typically determined from a suite of tests performed at different strain-rates and temperatures [11-12], however, as of the writing of this manuscript, no Zerilli-Armstrong parameters for magnesium alloys have been reported. For the purpose of this study, we empirically fit the curve using parameters of similar magnitude to those found in Ref. [11] to our experimental data ($c_3 = 0.005\ K^{-1}$, $c_4 = 0.0008\ K^{-1}$, and a c_2 value of 50 MPa, to obtain results comparable in magnitude to our experimental data). Figure 5 shows the data from Figure 4 for the AM60 magnesium alloy plotted with the Johnson-Cook, Cowper-Symonds and Zerilli-Armstrong constitutive material models normalized to the quasi-static reference stress in each equation. The figure shows that the Johnson-Cook and Zerilli-Armstrong models overestimate the compressive strength increase of AM60 at strain-rates up to approximately $500s^{-1}$. The Cowper-Symonds model accurately characterizes the effects of the strain-rate on the compressive strength of AM60, and is determined to best fit the experimental data. While the Cowper-Symonds equation is limited to strain-rates less than $1000s^{-1}$ [5], as it lacks a parameter to account for the increase of work-hardening due to strain-rate effects, it is sufficient for the range of strain-rates investigated here ($100s^{-1}$-$500s^{-1}$), and typically experienced in automotive crashes.

Conclusions

This work investigates the compressive strain-rate effects on the mechanical properties of sand-cast AE44, AZ91 and AM60 and die-cast AM60 magnesium alloys using uniaxial compression and impact testing. The results from this work indicate that the lower strain-rate sensitivity of the sand cast alloys may result from the larger grain sizes. Further, there was no indication of any strain-rate effects for the rare-earth magnesium alloy, AE44. It was determined that the Cowper-Symonds constitutive material model best characterizes the strain-rates effects of the HPDC-AM60 alloy at strain-rates between $150s^{-1}$ and $500s^{-1}$. At these strain-rates, a greater number of shear cracks and shear banding develop leading to an increase in the absorbed fracture energy of the material.

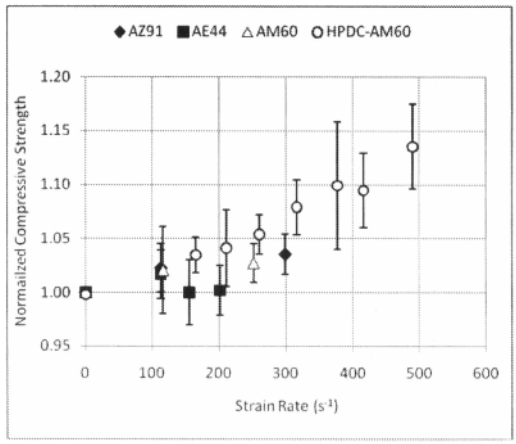

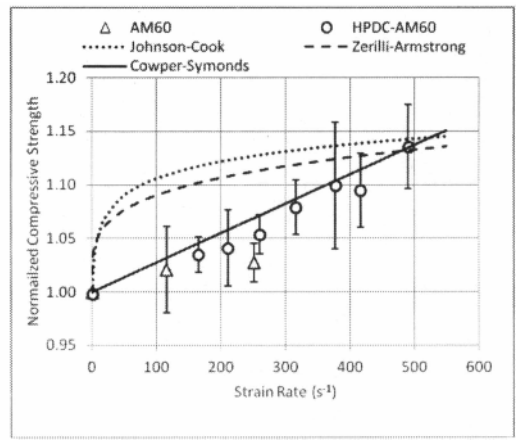

Figure 4 (left): Impact compressive strength normalized to the quasi-static compressive strength plotted as a function of the strain rate for each sand cast alloy: AE44, AZ91 and AM60, and for HPDC-AM60.
Figure 5 (right): Constitutive material models plotted to characterize the compressive strengths in Figure 4 of sand cast and HPDC-AM60.

Acknowledgements

The authors of this work would like to gratefully acknowledge the significant contributions of Mr. Junming Li in performing the casting experiments. We are grateful as well to Meridian Lightweight Technologies Inc. for access to the materials, equipment and facilities that made this work possible and the Resource for the Innovation of Engineering Materials (RIEM) program funded by CANMET (Canada Centre for Mineral and Energy Technology), a Natural Resources Canada laboratory. This research is funded by Meridian Lightweight Technologies Inc. and the AUTO21 Network of Centres of Excellence, an automotive research and development program focusing on issues relating to the automobile in the 21st century. AUTO21, a member of the Networks of Centres of Excellence of Canada program is funded by the Natural Sciences and Engineering Research Council (NSERC), the Social Science and Humanities Research Council (SSHRC) and multiple industry and government partners.

References

1. T. Rzychoń, and A. Kiełbus, "The influence of wall thickness on the microstructure of HPDC AE44 alloy," *Archives Mater. Sci. Eng.*, 28 (8) (2007), 471-474.
2. C.A. Newland, and M.T. Murray, "Strain rate dependent behaviour of Magnesium-based alloys," *Proceedings of the First Australasian Congress on Applied Mechanics: ACAM-96*, ed. R.H. Grzebieta (Barton, ACT, Australia: Institution of Engineers, Australia, 1996), 73-76.
3. T.K. Aune et al., "Behavior of die cast Magnesium alloys subject to rapid deformation," *SAE 2000 World Congress*, (2000) TP#: 2000-01-1116.
4. T. Abbott, M. Easton, and R. Schmidt, "Magnesium for crashworthy components," *Magnesium Technology 2003*, ed. H.I. Kaplan (Warrendale, PA: The Minerals, Metals and Materials Society, 2003), 227-230.
5. W.Q. Song, P. Beggs, and M. Easton, "Compressive strain-rate sensitivity of magnesium-aluminum die casting alloys," *Mater. Design*, 30 (2009), 642-648.
6. H.J. Choi et al., "Deformation behavior of magnesium in the grain size spectrum from nano- to micrometer," *Mater. Sci. Eng. A*, A527 (2010), 1565-1570.
7. N. Stanford et al., "Effect of Al and Gd solutes on the strain rate sensitivity of magnesium alloys," *Metall. Mater. Trans. A*, 41A (2010) 734-743.
8. *LS-DYNA Keyword User's Manual*, Version 971, (Livermore, CA: LSTC, 2007).
9. G.R. Johnson, and W.H. Cook, "A constitutive model and data for metals subjected to large strains, high strain rates and high temperatures," *Proc. 7th Inter. Symposium Ballistics* (ADPA, 1983), 541.
10. G.R. Cowper, and P.S. Symonds, "Strain hardening and strain-rate effects in the impact loading of cantilever beams," *Brown University Division of Applied Mathematics Report 28* (1957).
11. F.J. Zerilli, and R.W. Armstrong, "Dislocation-mechanics-based constitutive relations for material dynamics calculations," *J. Appl. Phys.*, 61 (5) (1987), 1816-1825.
12. F.J. Zerilli, and R.W. Armstrong, "Constitutive equation for HCP metals and high strength alloy steels," *ASME AD-Vol. 48*, (New York, NY: American Society of Mechanical Engineers, 1995), 121-126.
13. W. Altenhof, and W. Ames, "Strain rate effects for aluminum and magnesium in finite element simulations of steering wheel armature impact tests," *Fatigue Frac. Eng. Mater. Struct.*, 25 (2002), 1149-1156.
14. J.P. Weiler, J.T. Wood, and I. Basu, "Process-structure-property relationships for cast magnesium alloys," *Accepted to THERMEC 2011.*
15. J.T. Wood, J.P. Weiler, and I. Basu, "Study of solidification of magnesium alloys during high pressure die casting," *Accepted to THERMEC 2011.*
16. N.D. Alexopoulos, and A. Stylianos, "Impact mechanical behaviour of Al-7Si-Mg (A357) cast aluminum alloy. The effect of artificial aging," *Mater. Sci. Eng. A*, A528 (2011), 6303-6312.